pubs.acs.org/Biomac

Article

Remendable Cross-Linked Alginate/Gelatin Hydrogels Incorporating Nanofibers for Wound Repair and Regeneration

Changgi Hong,[#] Haeun Chung,[#] Gyubok Lee, Dongwoo Kim, Zhuomin Jiang, Sang-Heon Kim,* and Kangwon Lee*

Cite This: https://doi.org/10.1021/acs.biomac.4c00406

Read Online

ACCESS | Metrics & More | Article Recommendations | Supporting Information

ABSTRACT: Wound dressings made from natural-derived polymers are highly valued for their biocompatibility, biodegradability, and biofunctionality. However, natural polymer-based hydrogels can come with their own set of limitations, such as low mechanical strength, limited cell affinity, and the potential cytotoxicity of cross-linkers, which delineate the boundaries of their usage and hamper their practical application. To overcome the limitation of natural-derived polymers, this study utilized a mixture of oxidized alginate and gelatin with 5 mg/mL polycaprolactone (PCL):gelatin nanofiber fragments at a ratio of 7:3 (OGN-7) to develop a hydrogel composite wound dressing that can be injected and has the ability to be remended. The in situ formation of the remendable hydrogel is facilitated by dual cross-linking of oxidized alginate chains with gelatin and PCL/gelatin nanofibers through Schiff-base mechanisms, supported by the physical integration of nanofibers, thereby obviating the need for additional cross-linking agents. Furthermore, OGN-7 exhibits increased stiffness (γ = 79.4−316.3%), reduced gelation time (543 ± 5 to 475 ± 5 s), improved remendability of the hydrogel, and excellent biocompatibility. Notably, OGN-7 achieves full fusion within 1 h of incubation and maintains structural integrity under external stress, effectively overcoming the inherent mechanical weaknesses of natural polymer-based dressings and enhancing biofunctionality. The therapeutic efficacy of OGN-7 was validated through a full-thickness *in vivo* wound healing analysis, which demonstrated that OGN-7 significantly accelerates wound closure compared to alginate-based dressings and control groups. Histological analysis further revealed that re-epithelialization and collagen deposition were markedly enhanced in the regenerating skin of the OGN-7 group, confirming the superior therapeutic performance of OGN-7. In summary, OGN-7 optimized the synergistic effects of natural polymers, which enhances their collective functionality as a wound dressing and expands their utility across diverse biomedical applications.

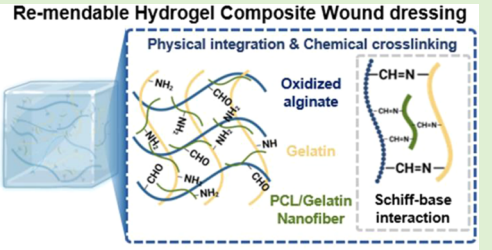

1. INTRODUCTION

Wound dressings consisting of natural-derived polymers are a cost-effective option that provides numerous biological advantages, such as being biocompatible, biodegradable, nontoxic, and swellable and causing less inflammation.[1] Despite these advantages, every natural polymer-based hydrogel has its own set of limitations, including a low mechanical modulus, limited cell affinity, and the potential cytotoxicity of cross-linkers.[2] These limitations clearly outline the restrictions on their own use and hamper their practical application, but they also result in a considerable economic loss for the healthcare industry, given the high demand for more durable and adaptable wound dressing solutions.[3] By optimizing the synergistic effects of combining distinct natural polymers, there is significant potential to access a broad market for advanced biomaterials that capitalize on the inherent biological properties of these natural polymers, which enhances their collective functionality and expands their utility across diverse biomedical applications.

Remendable hydrogels, which are synthesized using reversible dynamic covalent cross-linking, have emerged as a promising advancement in the field of natural polymer-based hydrogel wound dressings. These hydrogels possess desirable characteristics such as injectability, moldability, attachability, and durability, making them a preferred choice for the next-generation wound dressings.[4,5] Remendable properties can be demonstrated with natural polymers by the incorporation of functional groups into their backbones via chemical mechanisms. The substance has the capability to be injected at the wound site using a syringe and effectively attach to the irregular surface of the wound, hence improving the adhesion between the skin and the dressing.[6,7]

Oxidized alginate (OA) and gelatin have gained recognition in the field of developing remending natural hydrogels owing to their inherent elasticity and adaptability.[8,9] Balakrishnan et

Received: March 26, 2024
Revised: June 13, 2024
Accepted: June 13, 2024

al. successfully combined OA with gelatin to create an injectable and remendable hydrogel that promotes cartilage regeneration without inducing substantial inflammatory or oxidative stress responses.[8] Sarker et al. observed an enhanced rate of bone regeneration after embedding hydroxyapatite in an OA−gelatin hydrogel.[10] Encapsulating hydroxyapatite granules in an OA−gelatin hydrogel matrix improved osteoconductivity, osteointegration, swelling control, and structural stability.

Nevertheless, the remendable hydrogel formed by the interaction of OA and gelatin exhibited fragility and susceptibility to damage when utilized as a wound dressing, mostly attributed to the insufficient cross-linking of the Schiff-base interaction. Previous studies have investigated the integration of nanoparticles with hydrogel solutions in order to augment the mechanical rigidity of remendable hydrogels.[11−14] The inclusion of these particles during the gelation phase of the hydrogel serves to strengthen the internal cohesion and general stability of the polymers.

The present study employed oxidized alginate, gelatin, and functionalized PCL/gelatin nanofiber fragments in order to fabricate an injectable, remendable, and mechanically rigid hydrogel composite wound dressing with enhanced properties. Nanofibers are advantageous materials with a high surface area-to-volume ratio and excellent physical properties, offering versatile applications depending on their composition and functional groups.[15,16] The incorporation of nanofibers into the hydrogel matrix functions to enhance its mechanical properties and reinforce its structural integrity.[17,18] The hydrogel is physically conjugated by the nanofiber, and the gelatin component within the nanofiber is broadly dispersed and participates in the Schiff-base reaction with OA, which facilitates the gelation process of the hydrogel.[19] The incorporation of nanofibers allowed for the development of a hydrogel wound dressing that demonstrated enhanced mechanical properties while maintaining the desirable remendability of hydrogels, resulting in a composite wound dressing that possesses ideal qualities for effective wound care.

Experiments were conducted to identify the optimal hydrogel composite composition ratio for use as a wound dressing. The diameter, cell affinity, gelation duration, mechanical enhancement, remendability, injectability, and swelling ratio of nanofibers were assessed based on the PCL:gelatin composition of the nanofiber samples of 10:0 (P10G0), 9:1 (P9G1), and 7:3 (P7G3). The biocompatibility of the hydrogel composite was subsequently assessed by a cytotoxicity experiment employing fibroblasts. The hydrogel composite's therapeutic efficacy was evaluated using an *in vivo* full-thickness wound model. The utilization of the newly developed remendable wound dressing demonstrated enhanced wound closure rate and re-epithelialization in comparison to both the alginate hydrogel and the control group.

2. EXPERIMENTAL SECTION

2.1. Materials. Sodium alginate (80−120 cP) was purchased from Wako Pure Chemistry Industries Ltd. (Osaka, Japan); gelatin type A from porcine skin, polycaprolactone (PCL, M_n = 80,000), 2,2,2-trifluoroethanol (2,2,2-TFE), hexamethylenediamine 99.8%, sodium tetraborate decahydrate (ACS reagent, >99.5%), 4′,6-diamidino-2-phenylindole, and sodium (meta)periodate were purchased from Sigma-Aldrich (St Louis, MO). Alexa Fluor 488 phalloidin was purchased from Invitrogen. Acetic acid (glacial, 99.5%) and sodium hydroxide solution (1 mol/L) were obtained from Samchun (Gyeonggi-do, Korea). 4% paraformaldehyde was acquired from Biosesang (Gyeonggi-do, Korea). Dojindo Laboratories provided the Cell Counting Kit-8 (CCK-8) (Tokyo, Japan). Fetal bovine serum (FBS) was purchased from CellSera (Rutherford, NSW, Australia). Dulbecco's phosphate-buffered saline (DPBS) and Dulbecco's modified eagle medium (DMEM) were supplied by Welgene (Seoul, Korea). LIVE/DEAD was obtained from Thermo Fisher (Waltham, MA).

2.2. Fabrication of a Remendable Hydrogel Composite. *2.2.1. Ring-Opening Oxidation of Sodium Alginate.* The dialdehyde functionalization of sodium alginate via periodate mediation was conducted in accordance with the protocol described in a previous publication.[20] A stock solution of 0.25 g/mL sodium alginate was prepared in 100% ethanol, and a stock solution of 0.12 g/mL sodium periodate was prepared in deionized water. The sodium periodate solution was then added drop by drop into the sodium alginate solution with continuous stirring in the dark over 6 h at 25 °C. After the completion of the reaction, the resulting solution was dialyzed in distilled water for 3 days to remove the unreacted residual sodium periodate. Following lyophilization over 3 days, the oxidized alginate (OA) was stored at 4 °C for future use.

A hydroxylamine hydrochloride assay was performed in order to evaluate the degree of functionalization of oxidized alginate.[8] First, OA solution at 5 mg/mL was prepared in 0.25 N hydroxylamine hydrochloride with methyl orange as a color indicator and stirred for 2 h at 25 °C. Next, the resulting solution was titrated against a 0.1 M sodium hydroxide solution until the solution's color changed from orange to red. The equation was used to determine the degree of functionalization.[21]

$$\mathrm{DOF}(\%) = (M_{\text{sodium alginate}} M_{\mathrm{NaOH}} (V_{\mathrm{OA}} - V_{\text{control}})/m) \times 100$$

where m: mass of sodium alginate (g), $M_{\text{sodium alginate}}$: molecular weight of the sodium alginate repeating unit (198 g/mol), M_{NaOH}: molecular weight of sodium hydroxide (g/mol), and $V_{\mathrm{OA}} - V_{\text{control}}$: the consumed amount of sodium chloride (L).

2.2.2. Preparation of Electrospinning Solutions. The process of synthesizing nanofibers using electrospinning was conducted in accordance with the protocol described in a prior publication.[22] First, 10% (w/v) PCL and 10% (w/v) gelatin were dissolved separately in 2,2,2-trifluoroethanol overnight at room temperature with continual stirring. Subsequently, a 3% (v/v) acetic acid solution was introduced into the electrospinning solution in order to achieve a uniform dispersion of gelatin. Following complete dissolution of the polymers in a solution that exhibited transparency, solutions were subsequently combined in varying volume gradient ratios of 10:0 (P10G0), 9:1 (P9G1), and 7:3 (P7G3). Subsequently, the resulting mixture was subjected to electrospinning for 48 h.

2.2.3. Synthesis of Short Electrospun Nanofibers. Each PCL/gelatin solution was injected into a 3 mL plastic syringe fitted with a 25G needle in accordance with the protocol described in a prior publication.[23] During the electrospinning procedure, a consistent distance of 15 cm was maintained between the collector and the needle tip. The feed rate was set at 0.3 mL/h, and a voltage of 13 kV was applied for a duration of 2 h at 37 °C. Initially, a drum collector enveloped in aluminum foil was subjected to a rotational velocity of 3000 rpm in order to accumulate nanofibers in an aligned manner. Subsequently, the nanofibers are submerged in cold, deionized water overnight in order to eliminate any residual solvent or salt. Deionized water was kept at a temperature below 4 °C in order to minimize the dissolution of gelatin from the PCL/gelatin nanofiber.

The nanofiber extracted from the foil was divided into 1 mm^2 squares and further fragmented using tweezers. To minimize size variation during the fragmentation process, the nanofibers were fragmented with consistent fragmentation time and frequency, accompanied by continuous microscopic monitoring. Next, sizable fragments were subjected to centrifugation and subsequently fragmented once more to yield nanofibers with a homogeneous length.

Then, the nanofibers underwent freeze drying and were kept in a freezer until future use.[24] In order to assess the axial length of nanofiber fragments, they were dispersed in phosphate-buffered saline

https://doi.org/10.1021/acs.biomac.4c00406
Biomacromolecules XXXX, XXX, XXX−XXX

(PBS), photographed using a Zeiss Axio Vert1 A1 phase contrast microscope (Oberkochen, Germany), and assessed for length using ImageJ software (National Institutes of Health, Maryland).

2.2.4. Remendable Hydrogel Nanofiber Composite Synthesis. A stock solution of 10% (w/w) oxidized alginate in 0.1 M sodium tetraborate decahydrate was prepared by stirring until it turned transparent for 6 h at room temperature. A 10% (w/w) gelatin stock solution was prepared in PBS and stirred at 37 °C until a homogeneous solution was obtained. Then, equal volumes of oxidized alginate and gelatin stock solutions were combined at room temperature to produce a Schiff-base cross-linked oxidized alginate and gelatin remendable hydrogel.[25] In order to fabricate a hydrogel composite including the PCL/gelatin nanofiber (OGN), 10 mg/mL freeze-dried nanofiber was first introduced into the gelatin solution and subsequently mixed with an equal volume of OA under ambient conditions. Prior to hydrogel gelation, the hydrogel composite was sonicated to uniformly disperse the nanofiber.

2.3. Characterization of an Oxidized Alginate−Gelatin Nanofiber Hydrogel Composite. The hydrogel composite's components were evaluated by the utilization of a Fourier transform infrared (FT-IR) spectrometer (α, Bruker, MA). The FT-IR spectra of dehydrated alginate, oxidized alginate, gelatin, and PCL/gelatin nanofibers were acquired with a needle at a temperature of 25 °C in accordance with the protocol described in a prior publication.[26] The morphologies of various compositions of nanofibers and freeze-dried hydrogels were examined using a scanning electron microscopy (SEM) (SNE-4500 M, NanoImages, CA) needle in accordance with the protocol described in a prior publication.[22] The viscoelastic characteristics of scaffolds were evaluated by measuring the storage modulus (G') and loss modulus (G'') using an MCR 102 instrument (Anton-Paar, Australian Graz material) in accordance with the protocol described in a prior publication.[22,27] The storage modulus was measured by the implementation of a strain sweep test at a frequency of 1 Hz at a temperature of 20 °C. Additionally, an alternate step of strain sweep was conducted at the same frequency of 1 Hz. The amplitude oscillatory strain levels of hydrogels were altered in the range of 30−300% for OGN-9 and 400% for OGN-7.

2.3.1. Swelling Ratio and Gelation Rate. Initially, the samples OG and OGN were subjected to the process of freeze drying, following which their respective W_0 values were measured in accordance with the protocol described in a prior publication.[28] The freeze-dried hydrogel composites were subsequently immersed in PBS at 25 °C. At each time point, excess PBS was absorbed from the hydrogel's surface using filter paper and weighted in triplicate. The swelling ratio (SR) was defined as $(W_t - W_0)$ x $100/W_0$.[88]

Gelation time in response to the addition of nanofibers was determined as 1 mL of 10% OA, gelatin solution, and nanofibers (5 mg/mL) combined in a glass vial according to the procedure described in 2.2.4. Following a 1 min mixing period, the hydrogel composites were subsequently introduced into the vial by injection. A tube inversion test was conducted in order to ascertain the gelation duration under ambient conditions in accordance with the protocol described in a prior publication.[29]

2.3.2. Scanning Electron Microscopy. The sample preparation for scanning electron microscopy (SEM) is performed in accordance with the protocol described in a prior publication.[30] First, samples were fixed with a 4% paraformaldehyde solution for 2 h. The sample was then dehydrated using a gradient ethanol solution with concentrations of 70, 80, 90, and 100%. The dehydrated hydrogel was additionally desiccated using a freezing drier (Ilshin Bio Base, Korea) for a duration of 48 h. The desiccated specimen was coated with platinum using a sputter coater (SPI-module sputter coater; SPI Supplies, West Chester, PA) and examined using a scanning electron microscope (Tenoeo Volume Scope, FEI; Hillsboro, OR) at an acceleration voltage of 15 kV.

2.3.3. Remendability and Injectability. The difference in the remendability of the hydrogel was observed by the application of a staining reagent, resulting in the hydrogel being dyed blue in accordance with the protocol described in a prior publication.[31] The hydrogel, which had undergone gelation within the syringe, was divided into four equal parts and afterward positioned on a Petri plate. To explore the remendability of hydrogels, portions of both colored and noncolored hydrogels were joined together and allowed to make appropriate contact for 1 h at a temperature of 37 °C with PBS to avoid dehydration. Furthermore, an investigation was conducted to assess the injectability of the hydrogel composite, with the aim of determining its suitability for administration by a syringe into the wound site. The colored hydrogel composite solution was introduced into a syringe equipped with an 18G needle and subsequently administered onto a Petri plate.

2.3.4. Cell Culture. In order to conduct an *in vitro* examination of the hydrogel wound dressing, human fibroblasts (CCD-986sk cell line, Korean Cell Line Bank, Seoul, South Korea) at Passage 5 were cultivated within a 75T flask. The fibroblasts were cultured using medium composed of a mixture of high-glucose DMEM, 10% fetal bovine serum (FBS), and 1% penicillin−streptomycin (PS). The cells were subjected to incubation at a temperature of 37 °C inside an incubator with 5% CO_2. Fresh medium was replaced every 3 days.

2.3.5. Degree of Interaction with Fibroblasts. A nanofiber mesh was used as a scaffold for 2 days of fibroblast culture in order to compare cell affinity based on the gelatin component ratio. Changes in morphology, including elongation, migration, and proliferation, were observed. Using fluorescence images, the F-actin cytoskeleton and nuclei of cells were stained to visualize the morphology of the cells. Briefly, cells were fixed with 4% paraformaldehyde, permeabilized with 0.1% Triton X-100 (Aladdin, China), and blocked with a 4% bovine serum albumin (BSA) solution at 25 °C. After staining the cells against F-actin and nuclei, samples were washed in PBS and imaged using fluorescence microscopy (Axio Observer, Carl Zeiss, Oberkochen, Germany) to visualize changes in morphology, including elongation, migration, and proliferation of fibroblasts, cultured on nanofibers prepared using varying PCL:gelatin ratios.

2.3.6. Water Contact Angle. The contact angle of 8 μL of DI water on the PCL/gelatin nanofiber membrane surface was measured using a contact angle analyzer, SmartDrop (FEMTOFAB Co., Korea), in accordance with the protocol described in a prior publication.[23]

2.3.7. Cytocompatibility Assay. The experiment on cytotoxicity was carried out in an indirect manner, in accordance with the guidelines outlined in ISO 10993−12.[24] Hydrogel extracts were generated by immersing the hydrogel composite in nonserum-supplemented Dulbecco's modified Eagle medium (DMEM) at a concentration of 0.2 g/mL. This immersion was carried out for a duration of 24 h at 37 °C inside an incubator. The solution that was first separated underwent a dilution process in which it was mixed with an equal volume of nonserum-supplemented media. The cells were seeded into 96-well plates, and the diluted solution was administered, whereas the control group was exposed to only nonserum-supplemented media.

2.3.8. Cell Viability Assay. Human fibroblasts were cultured in 96-well plates at a density of 5×10^4 cells per well for 24 h. After removing the media by suctioning, the cells were subjected to incubation for a period of 1 to 4 days. This incubation took place in a humidified incubator maintained at a temperature of 37 °C in an atmosphere containing 5% CO_2. The assessment of cellular viability was then conducted using the Cell Counting Kit-8 (CCK-8) at two specific time intervals, namely 1 and 4 days. Each well was immersed in a CCK-8 solution and subjected to 2 h incubation period. The optical density (OD) of each well was determined at a wavelength of 450 nm using a microplate reader (Synergy H1, BioTek, VT).

2.3.9. Live/Dead Assay. Human fibroblasts were seeded at 3×10^4 cells per well on 24-well plates for 24 h before the experiment. The extract solution was processed in a manner consistent with the cell viability assay, and afterward, the LIVE/DEAD viability/cytotoxicity assay was employed to assess cell viability at each designated time interval. Cells were subjected to a reagent treatment for a duration of 45 min under dark conditions at a temperature of 27 °C. The fibroblasts were seen under a fluorescent microscope (Azio Observer Z1, Carl Zeiss, Oberkochen, Germany) following a DPBS wash.

2.4. *In Vivo* Test. *2.4.1. Animal Care.* Male BALB/c mice, aged 7 weeks, were obtained from Orient Bio Inc. (Seongnam, South Korea).

https://doi.org/10.1021/acs.biomac.4c00406
Biomacromolecules XXXX, XXX, XXX−XXX

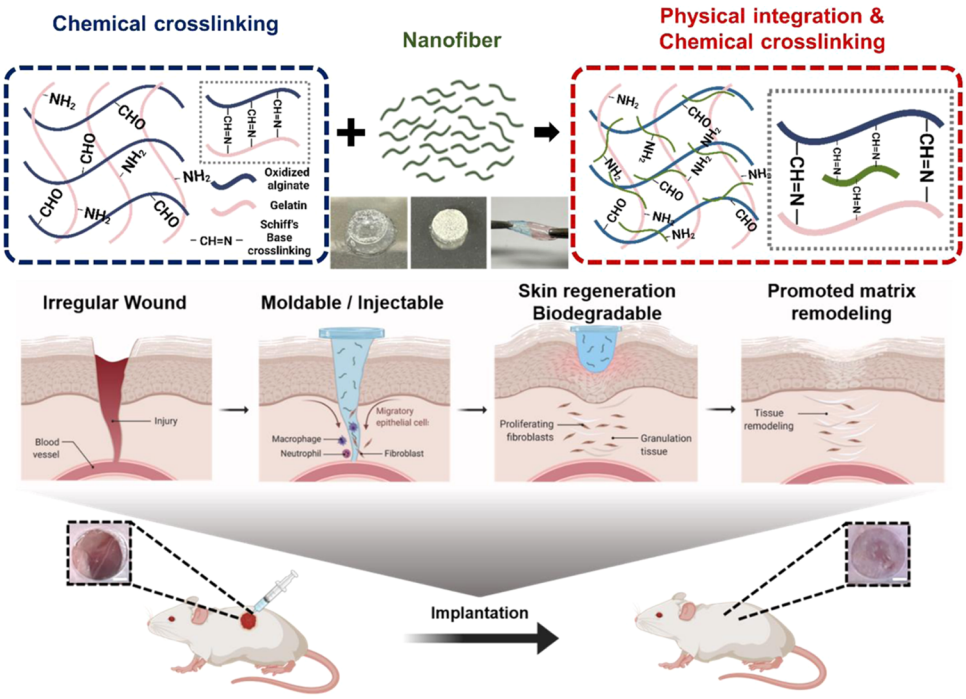

Figure 1. Schematic illustration of remendable hydrogel composite wound dressing OGN-7 for wound regeneration. A nanofiber with a composition of PCL:gelatin ratio of 7:3 was included in the gelation process at a concentration of 5 mg/mL. This addition served as both a physical support and a chemical cross-linker, improving the mechanical properties of the hydrogel as a wound dressing. Scale bar = 2 mm. The figures were generated using the online platform Biorender.com.

The mice were given a week of acclimation prior to undergoing any surgical procedures. Throughout the study, the mice were given unlimited access to food and water and were housed in a room maintained in a controlled environment with a temperature of 25 °C and a 12 h light/dark cycle. The International Animal Care and Use Committee of the Korea Institute of Science and Technology has granted approval for conducting animal research related to wound healing under the reference number KIST-2022−067.

2.4.2. Surgical Procedure and Implantation of Scaffolds. Prior to the surgical procedure, the mice went through isoflurane inhalation to induce anesthesia and subsequently underwent shaving. In order to establish a model for wound splinting, full-thickness skin incisions of 8 mm diameter were made along the dorsal area of each mouse using an 8 mm biopsy punch. Krazy glue was employed to adhere silicon ring supports to the periphery of the wound with the intention of preventing contraction of the wound. A total of 18 mice were randomly allocated to one of three groups. Mice were assigned to one of three groups: the control group, the group receiving alginate hydrogel alone, or the group receiving cylinders of OGN-7 with a diameter of 10 mm. The scaffold's outside borders were carefully inserted beneath the incisions. Subsequently, the wounds were appropriately treated using Tegaderm (3 M Healthcare) as a bandage and dressing. Skin tissues were collected for histological analysis at days 7 and 14 postsurgery.

2.4.3. Macroscopic Evaluation and Wound Closure Rate. The wound healing progression in each group was assessed by capturing photographs of the wound locations on days 0, 3, 7, 10, and 14. The size of the wounds was determined using ImageJ (National Institutes of Health, Maryland). The rate of wound closure was determined using the formula $(A_0 - A_t)/A_0 \times 100\%$, where A_0 represents the initial area of the wound and A_t represents the area of the wound at a given time point, t.

2.4.4. Histological Evaluation. Following euthanasia, the skin tissue was collected by incision and fixed with 4% paraformaldehyde. Tissue samples were dehydrated in increasing concentrations of ethanol, incubated in xylene, and prepared into paraffin blocks. Sections of 10 μm-thick paraffin sections were cut, deparaffinized, and rehydrated. The prepared samples were stained with hematoxylin and eosin and Masson's trichrome stain solution for histological analysis. The tissue sections were photographed using a slide scanner (EasyScan, Motic, Hong Kong).

2.4.5. Immunofluorescent Analysis. Skin tissue was collected for the purpose of conducting immunofluorescent analysis on days 7 and 14 postsurgery. Paraffin sections of 4 μm thickness were made, deparaffinized, rehydrated, and incubated in the target retrieval solution for antigen retrieval (Dako, Denmark). The prepared slides were then blocked in blocking solution (2% BSA + 0.1% Triton X-100) for 1 h, incubated with primary antibodies diluted in blocking solution at 1:100 overnight at 4 °C, and then treated with secondary antibodies diluted in blocking solution at 1:500 for 2 h at 25 °C. Stained slides were visualized using a confocal microscope (Zeiss LSM 700, Zeiss, Oberkochen, Germany). The antibodies used in this paper are summarized in Figure S1.

2.5. Statistical Analysis. The experiments were performed in triplicate, and the results have been presented as the mean ± standard deviation. The data analysis was performed using GraphPad Prism version 8. The error bars represent the standard deviation. The t test, or one-way ANOVA, was employed to assess statistical significance, with a significance level of 0.05. P values below this threshold were considered to indicate statistical significance.

2.6. Literature Search. An extensive electronic literature search was performed on four databases: PubMed and Web of Science Core Collection (Clarivate) to identify articles published past the year 2000. This search utilized a complex set of search terms that covered various categories, including types of dressings, specific dressing ingredients, wound classifications, and specific keywords. Some examples of these terms are "alginate," "oxidized alginate," "gelatin," "remendable," and "nanofiber," among others.

3. RESULTS AND DISCUSSION

3.1. Synthesis and Characterization of Injectable Hydrogel Composites. The composition of the OGN hydrogel composite wound dressing includes oxidized alginate, gelatin, and nanofibers of PCL/gelatin (Figure 1). Alginate is

https://doi.org/10.1021/acs.biomac.4c00406
Biomacromolecules XXXX, XXX, XXX−XXX

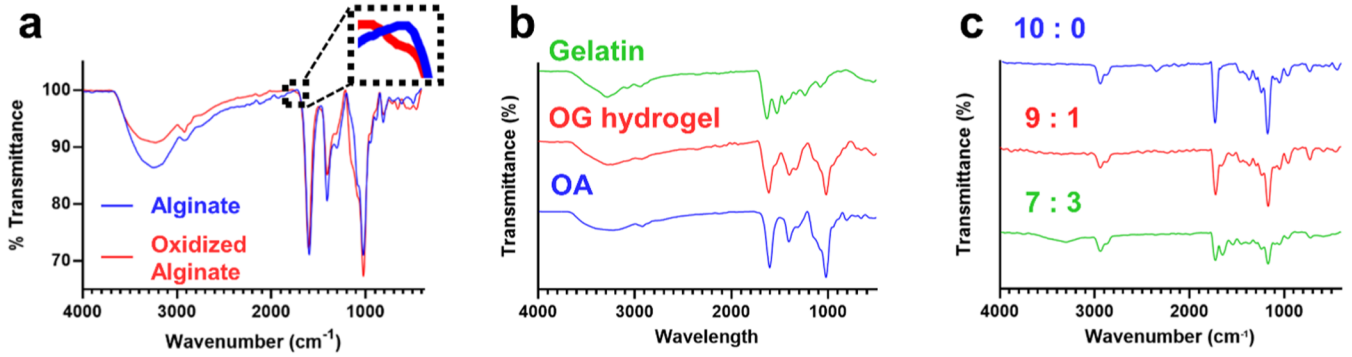

Figure 2. FT-IR spectra of alginate and oxidized alginate (a); oxidized alginate, gelatin, and OG hydrogel (b); and changes in the characteristic peak of a nanofiber in response to a concentration gradient (c).

commonly utilized in cell regeneration and drug delivery research due to its rigidity, bioinert properties, low toxicity, and ease of manufacturing.[32] The incorporation of dialdehyde functional groups into the polymer chain of alginate by oxidation enables its interaction with compounds that include amine groups in their backbone, such as gelatin and chitosan. The aforementioned reaction also serves to enhance the biocompatibility and biodegradability properties, which are crucial factors to consider in the field of tissue transplantation.[33] Gelatin is obtained by the process of collagen hydrolysis, and it shares similar biological properties with collagen, which is the primary constituent of skin. The presence of arginine−glycine−aspartic acid (RGD) sequences, which are often present in collagen, confers a high degree of efficacy for the purposes of cell adhesion, proliferation, and migration. Moreover, it has a notable abundance of glycine, proline, and hydroxyproline residues, which contribute to the facilitation of soft tissue regeneration and the process of wound healing.[34] Polycaprolactone (PCL) is a synthetic linear hydrophobic polymer with high tensile strength, biodegradability, and simplicity of manufacturing. When PCL is subjected to the electrospinning process to form nanofibers, it exhibits a notable surface-to-volume ratio, which in turn contributes to the enhancement of the scaffold's stiffness by establishing a physical framework.[35] Nevertheless, the hydrophobic nature of PCL presents a challenge in terms of its biocompatibility, hence rendering it inappropriate for biomaterials that require cellular interactions. In order to mitigate the inherent drawbacks of PCL, the researchers employed the technique of electrospinning in conjunction with gelatin to enhance its biocompatibility.[26] The augmentation of cell affinity in nanofibers and the subsequent improvement in their suitability for tissue engineering are achieved without compromising the physical characteristics of the nanofibers.[36,37]

The oxidation of alginate with sodium periodate resulted in the formation of dialdehyde groups on the backbone through ring opening. The hydroxylamine hydrochloride assay was conducted in order to quantify the extent of functionalization of oxidized alginate. The substitution rate of oxidized alginate, as determined using titration with 0.1 M sodium hydroxide, was found to be 39.6% (data not shown). The substitution rate of 39.6% provided a balanced approach, ensuring robust cross-linking while maintaining the mechanical properties and biocompatibility required for our application, as reported in previous papers.[38−42]

FT-IR analysis was conducted to ascertain the production and distribution of functional groups in the hydrogel and nanofiber (Figure 2). The emergence of a newly generated signal at a wavenumber of 1715 cm^{-1} in the oxidized alginate suggests the formation of an aldehyde functional group (−C═O) during the aforementioned procedure (Figure 2a).[41] The band's weakness can be attributed to the hemiacetal synthesis occurring between the free aldehyde groups and hydroxyl groups on neighboring uronic acid subunits.[43]

The gelation process was verified by observing a shift in the peak positions of the oxidized alginate/gelatin (OG) hydrogel, gelatin, and OA spectra in the FT-IR analysis (Figure 2b). It was observed that the absorption peak corresponding to the aldehyde group in OA at 1715 cm^{-1} vanished, whereas the peak associated with the −C═N double bond at 1620 cm^{-1} exhibited broadening. The broadening of this imine peak is attributed to the Schiff-base reaction occurring between the aldehyde moiety of OA and the amine moiety of gelatin. This chemical interaction leads to the creation of a hydrogel network, indicating the successful cross-linking of OA and gelatin in the OG hydrogel.[21]

Upon examination of the FT-IR spectra of nanofibers generated from varying ratios of PCL and gelatin (Figure 2c), it was observed that each nanofiber displayed an asymmetrical CH_2 stretching peak at 2949 cm^{-1} and a symmetrical CH_2 stretching peak at 2865 cm^{-1}. These peaks were found to correspond to the characteristic peaks of PCL. Additionally, the distinctive gelatin peaks, namely amide I and amide II, were identified at 1650 and 1540 cm^{-1}, respectively.[26] The apparent shifts in peak intensity as the PCL and gelatin compositions are modified indicate the successful generation of nanofibers by the implementation of a concentration gradient.

Following the preparation of materials for fabricating the hydrogel wound dressing, bare oxidized alginate−gelatin hydrogel (OG) and oxidized alginate−gelatin−nanofiber compositions (OGN-10, OGN-9, and OGN-7) were synthesized according to the PCL/gelatin composition in nanofibers. Initially, a hydrogel solution was prepared by dissolving OA in a phosphate-buffered saline (PBS) solution supplemented with 0.1 M tetraborate decahydrate. The presence of tetraborate decahydrate in the solution aids in the promotion of the Schiff-base reaction by effectively regulating the pH to a slightly alkaline level and establishing a complex with the hydroxyl group of OA.[44] Subsequently, a solution comprising freeze-dried nanofibers and gelatin was prepared, resulting in an opaque gelatin/nanofiber mixture. The nanofibers were dissolved in a 10% gelatin solution at a concentration of 10

https://doi.org/10.1021/acs.biomac.4c00406
Biomacromolecules XXXX, XXX, XXX−XXX

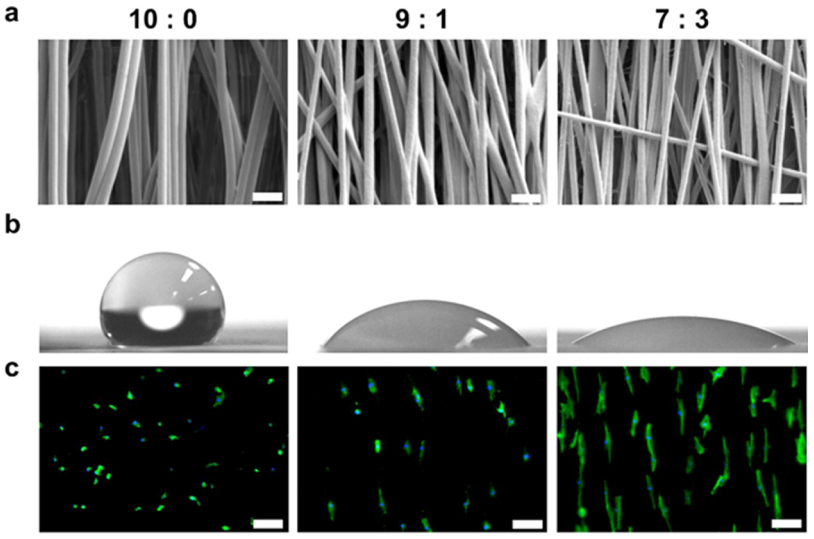

Figure 3. SEM images of PCL/gelatin nanofibers (scale bar = 1 μm) (a); contact angle measurements. Images of a water droplet on the surfaces of nanofibers (b); fluorescence images of human fibroblasts seeded on various ratios of PCL/gelatin nanofibers. Cell nuclei were stained with DAPI and the actin cytoskeleton (F-actin) with Alexa Fluor 488-labeled phalloidin (c) (scale bar = 100 μm).

mg/mL and uniformly dispersed throughout the solution using sonication. OA and OGN solutions with equal volumes were combined and subsequently solidified at room temperature using a cylindrical mold. Therefore, the in situ formation of a remendable hydrogel is achieved by cross-linking OA chains using gelatin and PCL/gelatin nanofibers through physical integration and chemical cross-linking mechanisms, eliminating the requirement for further cross-linking agents.

3.2. Determination of the Composition of the Nanofiber Suitable for the Wound Dressing. The determination of the optimal PCL:gelatin ratio for the nanofiber was based on the evaluation of numerous factors, including the gelation rate, swelling ratio, rheology, and remendability of the OGN. An increase in the gelatin content within the nanofiber leads to a corresponding enhancement in the extent of Schiff-base cross-linking within the hydrogel, resulting in an elevation of the hydrogel's modulus value. Furthermore, the heightened quantity of peptide sequences that engage with cells results in an upregulation of cell proliferation and migration. It was observed that nanofibrous fragments incorporated within a hydrogel matrix could serve as an artificial collagen fibril extracellular matrix, thereby facilitating early cell proliferation and differentiation and augmenting wound regeneration.[45]

On the contrary, when the electrospinning solution had a higher concentration of gelatin, it resulted in the occurrence of branching and beading during the electrospinning process. This, in turn, has the disadvantage of reducing the modulus of the nanofiber and negatively affecting the cell interaction.[46] Moreover, the swellability of hydrogels was diminished due to the inhibitory effect of stiff cross-linking, which hindered their ability to undergo swelling. Consequently, the experimental values for each element were derived based on the composition of the nanofiber. The optimal PCL-to-gelatin ratio was obtained by considering their respective properties.

3.2.1. Fabrication and Characterization of the Electrospun Nanofibers. A 10% solution of PCL and gelatin were combined in various ratios and electrospun to produce nanofibers. When the ratio of gelatin content exceeds 7:3, the electrospinning fluid exhibits a low viscosity, which poses challenges in achieving a uniform diameter and alignment of nanofibers throughout the electrospinning process. It has been demonstrated previously in our research that the production of nanofibers with irregular diameters occurs when the ratio of polycaprolactone (PCL) to gelatin exceeds 7:3.[22] Hence, the alteration in the physical characteristics of the remendable hydrogel was assessed by varying the PCL to gelatin ratio in the range of 10:0−7:3.

Scanning electron microscopy (SEM) was employed to examine the surface characteristics of the nanofibers produced using different compositions (Figure 3). The SEM images revealed that the nanofibers exhibited a uniform and smooth morphology, devoid of any bead-like or branched structures. Furthermore, it was observed that the diameter of the nanofibers decreased as the concentration of gelatin in the solution increased. This reduction in diameter can be attributed to a decrease in the overall viscosity of the solution.[26] The specific measurements obtained were as follows: for P10G0, the diameter was 402 ± 36 nm; for P9G1, the diameter was 334 ± 54 nm; and for P7G3, the diameter was 313 ± 45 nm (n = 30) (Figures 3a and S2).

Water contact angle analysis was conducted to ascertain the gelatin distribution on the nanofiber surface, taking the gelatin ratio into account (n = 3) (Figure 3b). Water contact angles of 129.0 ± 2.0, 52.9 ± 1.9, and 31.3 ± 2.0° were measured in nanofibers manufactured at ratios of 10:0, 9:1, and 7:3 PCL/gelatin, respectively, confirming that the water contact angle decreases as the ratio of hydrophilic gelatin increases (Figure S3). A decrease in the water contact angle was associated with the increased hydrophilicity of the surface, making it more suitable for use in wound dressings.[47]

The morphologies of fibroblasts cultivated for 48 h on different nanofibrous scaffolds were analyzed using Alexa Fluor 488-labeled phalloidin to confirm that gelatin added to nanofibers could be employed for cell activation or hydrogel cross-linking (Figure 3c). Fluorescence staining illustrates how fibroblasts were stimulated to grow on nanofiber scaffolds containing different amounts of gelatin. Fluorescent images of fibroblasts at each composition revealed that the gelatin content of the nanofibers promoted fibroblast elongation and

https://doi.org/10.1021/acs.biomac.4c00406
Biomacromolecules XXXX, XXX, XXX−XXX

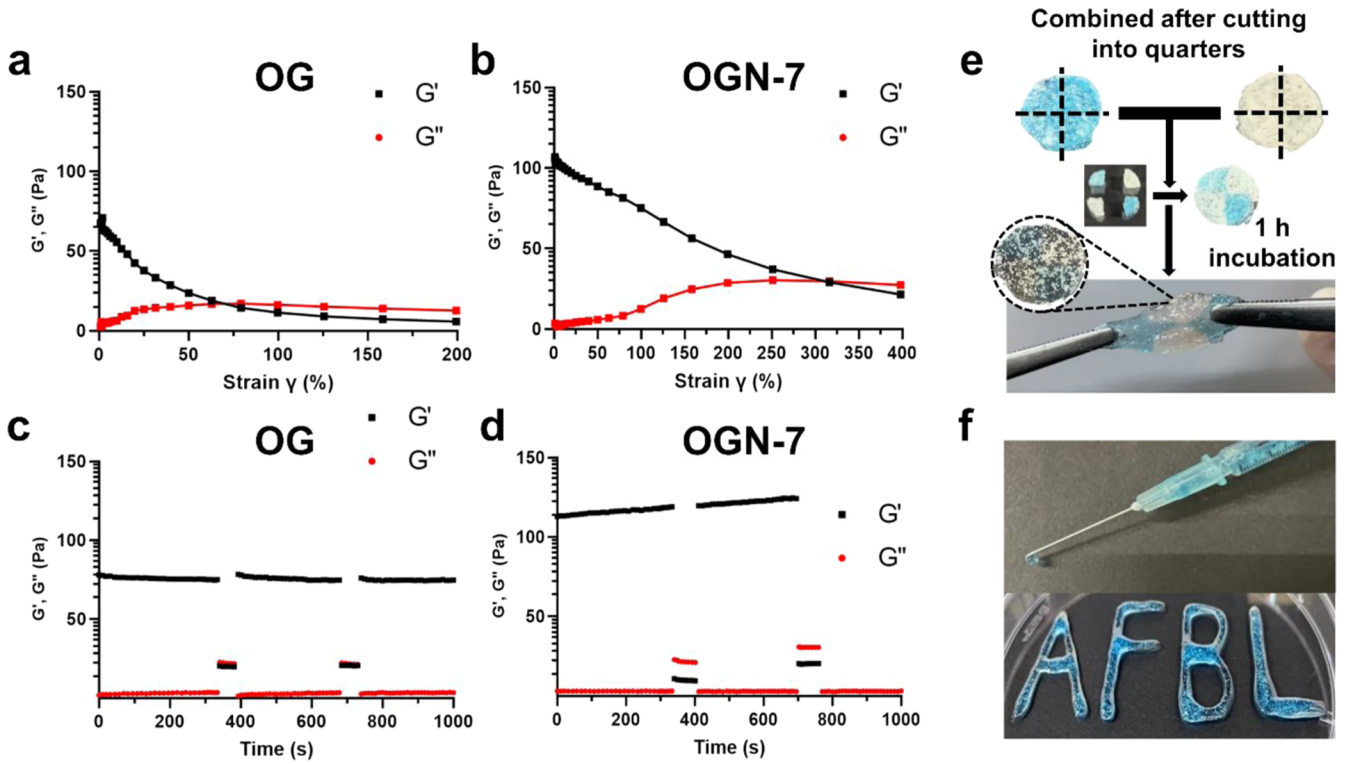

Figure 4. Strain amplitude sweep test of OG and OGN-7 (5 mg/mL) hydrogels at w = 1 Hz and 27 °C (a, b); alternative step strain test at w = 1 Hz and 27 °C, with amplitude oscillatory strain levels turning between γ = 30 and 100% for OG and γ = 30 and 400% for OGN-7 (c, d); remending procedure of OGN-7 hydrogels (e); and confirmation of injectability of OGN-7 by hand injection (f).

migration, whereas the fibroblasts did not proliferate by attaching to the surface of the PCL nanofibers; rather, they maintained their round shape during the early stages of cell seeding. In contrast, the condition with a ratio of 7:3 revealed a considerable upregulation of fibroblast proliferation and migration, demonstrating the presence of gelatin dispersed proportionately on the nanofiber surface depending on the composition.

The fragmented nanofiber possesses an axial length of 140.74 ± 24.55 μm, rendering it suitable for effective dispersion inside a hydrogel composite and facilitating its injection (n = 70) (Figure S4). The amine group present in the gelatin covering the nanofiber surface can undergo cross-linking with oxidized alginate via a Schiff-base reaction, significantly enhancing the stability of the hydrogel wound dressing.

3.2.2. Gelation and Swelling Rate. The gelation time refers to the period of time required for the completion of the cross-linking process. The gelation time of hydrogel composites was determined using the test tube inverting method (Figure S5).[48] As expected, the gelation time of OGN decreased as the concentration of gelatin in the nanofiber rose, resulting in a decrease in time from 513 ± 6.26 to 475 ± 4.56 s. With an increase in the gelation content of the nanofiber, a subsequent chemical cross-linking process took place during gelation. This led to a reduction in gelation time by 68 s compared to the original gel (543 ± 5.19 s) at OGN-7 (475 ± 4.56 s). These findings indicate that the nanofiber has the potential to function as a chemical cross-linker in the Schiff-base reaction. The incorporation of the nanofiber material significantly improved the gelation rate, and it is essential to note that PCL nanofibers, in the absence of gelatin, have the potential to improve the gelation rate of OGN-10. This suggests that the nanofiber itself can serve as a physical filler, facilitating more effective cross-linking between polymers during the gelation process.

Swelling tests were performed to establish the dressing's capability as a wound dressing capable of absorbing wound exudates and cleaning the site while preventing viral infection (n = 3) (Figure S6). The swelling kinetics and time-dependent swelling behaviors of hydrogels in a PBS buffer solution at 25 °C were examined. All hydrogels expanded rapidly and reached a high equilibrium point within 2 h. The swelling ratio of OG was the greatest (725 ± 14%), while that of OGN-7 was the lowest (506 ± 12%), indicating that the incorporation of nanofibers in the hydrogel composition resulted in enhanced cross-linking through the Schiff-base reaction inside the hydrogel matrix, thereby leading to a reduction in swelling. Nevertheless, it is noteworthy that all hydrogels exhibited a quick expansion, achieving a significant equilibrium state within a span of 2 h. This characteristic proved to be highly advantageous as it facilitated the efficient absorption of exudates from the wound surface, successfully restricting the proliferation of bacteria.[49]

The SEM image analysis has shown that both OG and OGN-7 possess significantly porous structures, with porosity values of 47.1 ± 1.2 and 42.1 ± 1.4%, respectively (n = 5) (Figure S7). The results are consistent with swelling analysis, suggesting that the addition of nanofibers to OGN-7 has led to enhanced mechanical integration, which is crucial for its mechanical modulus as a wound dressing.

3.3. Mechanical Properties of the Hydrogel. A strain amplitude sweep test was employed to evaluate the enhanced modulus of the hydrogel resulting from the incorporation of

https://doi.org/10.1021/acs.biomac.4c00406
Biomacromolecules XXXX, XXX, XXX−XXX

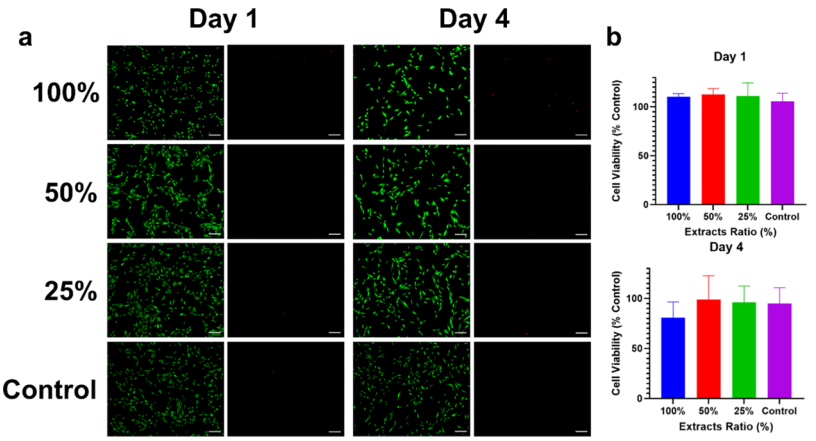

Figure 5. Cytotoxicity test of the OGN-7. Fluorescent images of fibroblasts treated with OGN-7 extracts for 1 or 4 days and subsequently stained with live (green) and dead (red) dyes (a) and cell viability of fibroblasts treated with the OGN-7 extract as determined using the CCK-8 assay on days 1 and 4 (n = 5) (b). Data are mean ± SD (scale bar: 100 μm).

nanofibers (Figures 4 and S8). The intersection of the G' and G'' values becomes evident with increasing strain applied to the hydrogel, suggesting the occurrence of shear thinning behavior and further supporting the injectability of hydrogels.[50] The point of intersection between G' and G'' is the critical strain threshold at which the hydrogel material reaches its maximal strain capacity. As anticipated, the mechanical properties of OGN-9 and OGN-7 hydrogels were found to be significantly improved when nanofibers composed of PCL/gelatin were incorporated (Figures 4a and S8a), while the OA hydrogel exhibited a strain tolerance of around 70%, rendering it unsuitable for use as a wound dressing (Figure 4b). Surprisingly, the addition of nanofibers increased the mechanical properties of OGN-9 and OGN-7 hydrogels by 250 and 300% of strain, respectively, indicating that the addition of PCL/gelatin nanofibers effectively enhanced the mechanical properties of OGN hydrogels, coordinating with the aforementioned results. In addition, as the concentration of gelatin in the nanofiber increased, the maximal strain that the hydrogel could withstand increased significantly, demonstrating its effectiveness as a chemical cross-linker.

Next, the hydrogel's remendability was evaluated using amplitude oscillatory analysis (Figures 4c,d and S8b). By applying a strain greater than the maximum strain previously measured for the hydrogel (100, 300, and 400% for OG, OGN-9, and OGN-7, respectively) and then continuously applying 30% relaxing strain, it was determined whether the hydrogel's original modulus could be restored upon denaturation.[27] The G' values of OG, OGN-9, and OGN-7 were significantly greater than their G'' values at 30% strain, indicating that these hydrogels possessed a rigid structure. When the maximal strain was reached, the hydrogel interconnection was disrupted and underwent a remending cycle in a 30% strain environment. Remarkably, the OGN-7 demonstrates that the hydrogel composite wound dressing retained a storage modulus 30% greater than the OG and maintained its initial modulus even after repeated denaturation. The modulus of the hydrogel exhibited a gradual rise following the stage of maximum strain, which can be attributed to the densification of the hydrogel. The findings of the study demonstrate that the incorporation of nanofibers into the hydrogel matrix contributes to the cross-linking mechanism and enhances the mechanical properties of the hydrogel wound dressing. The OGN-7 showed a notable ability to undergo remending, hence validating its efficacy as a hydrogel wound dressing. In order to evaluate remendability, the hydrogels exhibiting different colors were cut and placed next to each other (Figure 4e). Remarkably, the OGN-7 exhibited exceptional regenerative capabilities and underwent complete fusion subsequent to a 1 h incubation period at a temperature of 37 °C with PBS to avoid dehydration, maintaining its structural integrity even when subjected to external forces using forceps (Figure S9). Furthermore, the suitability of hydrogels for minimally invasive surgical procedures was enhanced, as demonstrated by their ability to be extruded and injected using a conventional medical syringe (Figure 4f). Remendability analyses demonstrate that hydrogels have exceptional remendability, rendering them potentially valuable for the treatment of diverse wounds and tissue regeneration.

The utilization of nanofibers in a PCL−gelatin ratio of 7:3 demonstrated optimal outcomes. This ratio facilitated a rapid gelation rate, enabling the material to conform efficiently to the contour of the wounded skin upon injection. Concurrently, it possesses the ability to withstand increased levels of strain while retaining an appropriate degree of swelling, enabling prolonged utilization as a dressing for wounds. Consequently, OGN-7 emerged as the most appropriate option for this research, and subsequent evaluations were conducted to assess its cytotoxicity and efficacy in promoting the healing of full-thickness wounds *in vivo*.

3.4. Cytocompatibility of the Composite Hydrogels.

The biocompatibility and cytotoxicity of OGN-7 were evaluated by the CCK-8 and Live/Dead assays on human fibroblasts (Figure 5). The experiment involved exposing fibroblasts to hydrogel extracts that were diluted in a stepwise manner (at concentrations of 100, 50, 25, 12.5%, and a control). Following incubation with the diluted hydrogel extract, fluorescence images of viable (green) and nonviable (red) cells were acquired (Figure 5a). The majority of the examined cells were live, with minor occurrences of dead cells detected across all experimental groups on days 1 and 4. Fibroblasts exhibited a typical structural appearance and demonstrated a significant level of viability, which was comparable to that observed in the control group. The cytotoxicity of hydrogel extracts was then assessed on both days 1 and 4 by the CCK-8 assay (n = 5) (Figure 5b). On days 1 and 4, the viability of all groups closely resembled that of the

https://doi.org/10.1021/acs.biomac.4c00406
Biomacromolecules XXXX, XXX, XXX−XXX

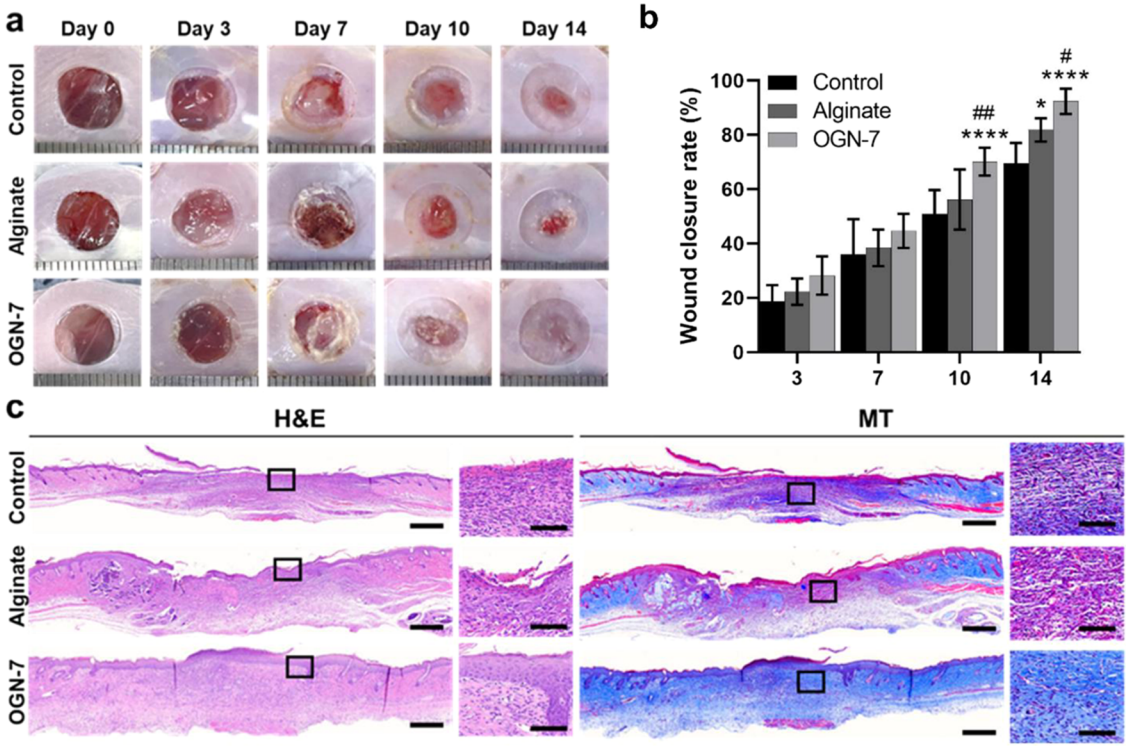

Figure 6. Digital photographs showing the size of the wound at each time point (a) and wound closure rate as determined for the control, alginate, and OGN-7 groups for 14 days of creating a full-thickness wound ($n = 6$) (b). Data are mean ± SD. Two-way ANOVA. *$p < 0.05$, ****$p < 0.0001$ against the control group; $^{\#}p < 0.05$, $^{\#\#}p < 0.01$ against the alginate group. H&E and MT-stained skin tissue was collected from the control, alginate, and OGN-7 groups on day 14 (c). Scale bar: 500 μm (inserts: 100 μm).

control group. These findings suggest that our hydrogel composite is biocompatible.

3.5. Full-Thickness Wound Healing *In Vivo*. A full-thickness wound model was generated on the dorsal side of a mouse and subsequently observed for a period of 0, 3, 7, and 14 days for wound closure (Figure 6). The evaluation was conducted to assess the healing efficacy of three different groups, namely the control group, the alginate group, and the OGN-7 group. Alginate, a constituent of OGN-7 and a representative natural polymer-based wound dressing material, possesses an adequate mechanical modulus along with biocompatibility, nontoxicity, and swelling ability and is already commercially available in wound dressing products.[51] Therefore, it was selected to confirm the enhanced efficacy of OGN-7 as a natural polymer-based wound dressing.

The results obtained from a digital photographic examination of wound size indicated that wounds treated with the standard alginate hydrogel and OGN-7 exhibited a more rapid wound closure rate than that in the control group (Figure 6a). It demonstrated that the promotion of cellular activity for wound healing has been enhanced in a moist environment, highlighting the essential role of hydrogel wound dressings in the field of tissue regeneration.[52] Furthermore, it was observed that the groups treated with dressings had little scab development on the surface of the wound, suggesting a reduced level of pain and a lower risk of scarring during the wound healing process.[53] The therapeutic effects of OGN-7 were confirmed by assessing the wound closure rates, with the OGN-7 group demonstrating the most effective wound healing, showing a significant difference from the alginate and control groups at days 10 and 14. The control group and the traditional alginate hydrogel group demonstrated partial wound closure rates of 67 and 80%, respectively. In contrast, the OGN-7 group displayed full wound closure at a rate of 95%, indicating considerably superior therapeutic efficacy compared to the other groups (Figure 6b) ($n = 6$).

Histological staining of skin as collected from three experimental groups was employed to assess the effectiveness of re-epithelialization and collagen deposition in regenerating skin during the wound healing process (Figure 6c). In comparison to the other groups, OGN-7 exhibited a notable acceleration in the process of wound healing, as demonstrated by the most substantial re-epithelialization and collagen deposition. The process of re-epithelialization, granulation, and collagen deposition takes place as the cells are recruited to the wound site.[54] The histological examination using H&E staining demonstrated that both the control group and the alginate group exhibited improper wound healing, as suggested by the lack of regeneration of the epithelial layer. Furthermore, it was seen that the thickness of the regenerated dermis layer exhibited an ascending trend, with the control group displaying the lowest thickness, followed by the alginate group and then by the OGN-7 group. In the OGN-7 group, rapid re-epithelialization was observed, as indicated by the thicker granulation tissue, whereas in the control and alginate groups, tissue production appeared to be ongoing, as indicated by the thinner granulation tissue. These findings suggest that the OGN-7 group successfully underwent the granulation process and progressed to the stage of collagen deposition. The findings obtained from the application of OGN-7 in both H&E and MT staining techniques were found to be comparable. The dermis layer generated in the OGN-7 group exhibited a prominent blue stain, suggesting increased collagen deposition, maturation, and extracellular matrix (ECM) remodeling. In

https://doi.org/10.1021/acs.biomac.4c00406
Biomacromolecules XXXX, XXX, XXX−XXX

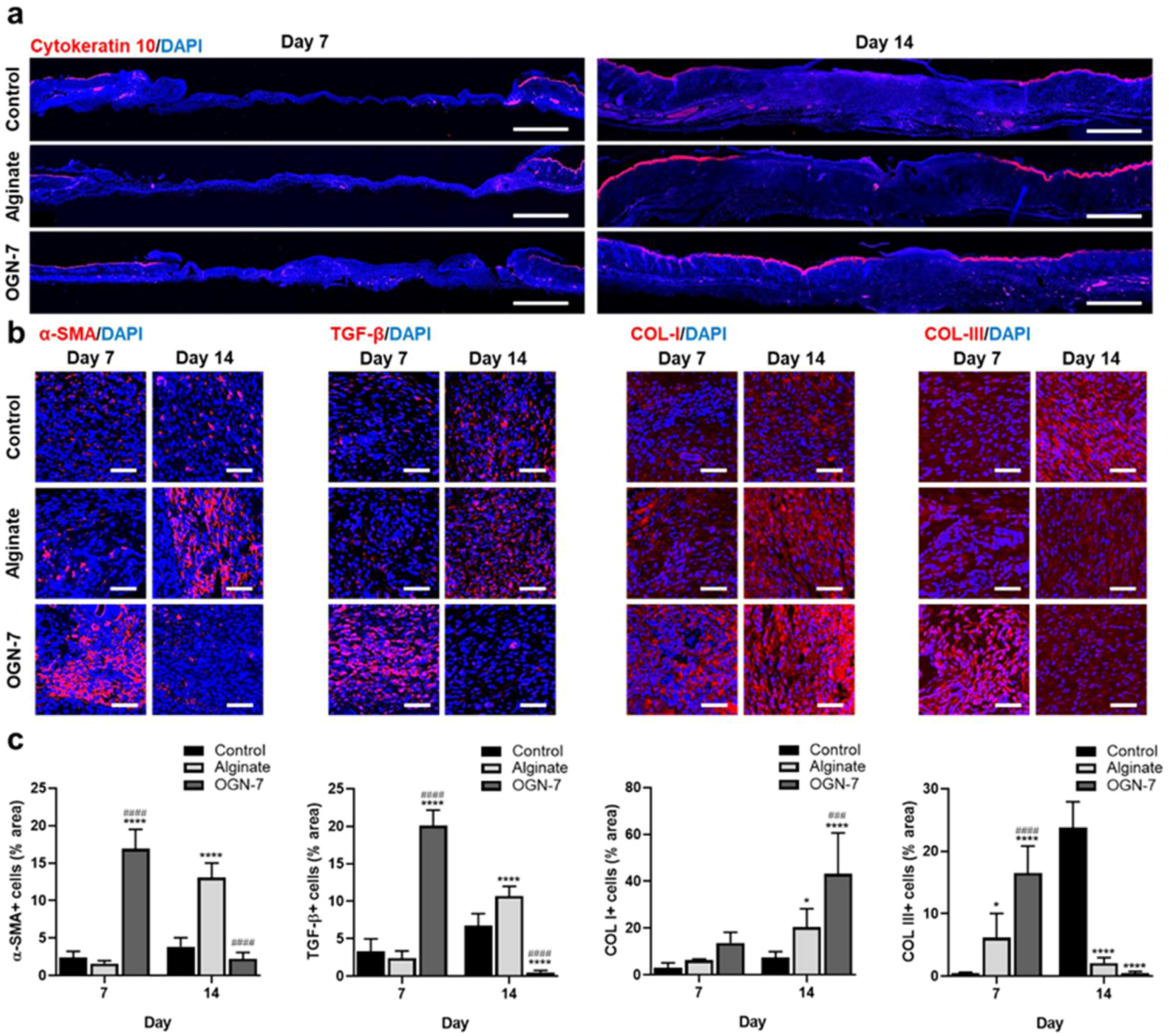

Figure 7. Immunofluorescent staining of cytokeratin 10 from full-thickness wounds as collected from the control, alginate, and OGN-7 groups on days 7 and 14 (a) Scale bar: 1 mm; Immunofluorescent staining of α-SMA, TGF-β, collagen type I, and collagen type III of full-thickness wounds collected on days 7 and 14 (b). Scale bar: 50 μm; quantification of α-SMA-, TGF-β-, collagen type I-, and collagen type III-positive cells in wounded skin as determined using ImageJ software (n = 5) (c). Data are mean ± SD $^{*}p < 0.05$, $^{****}p < 0.0001$ against the control group; $^{\#\#\#}p < 0.001$, and $^{\#\#\#\#}p < 0.0001$ against the alginate group.

contrast, both the control and alginate groups displayed considerably less blue stain, indicating a decreased collagen deposition in the granulation tissue. The results of this experiment suggest that the use of OGN-7 for enhancing skin regeneration in a manner that closely resembles the natural structure of the skin may offer potential benefits (Figure S10).

3.6. Immunofluorescent Analysis. Immunofluorescent staining of cytokeratin 10 and collagen types I and III was performed to determine the degree of maturation of regenerated skin tissue (Figure 7). Cytokeratin 10 serves as a marker for suprabasal differentiation, enabling the assessment of epidermal regeneration by differentiated keratinocytes in the re-epithelialization process.[55] In accordance with histological staining, it was seen that the OGN-7 group had greater migration of keratinocytes toward the wound bed at days 7 and 14, in comparison to the control and alginate groups (Figure 7a). The promotion of attachment, proliferation, and migration of keratinocytes was facilitated by the biocompatible constituents of OGN-7, resulting in upregulated cellular activity in the maturation of the epidermis.

The differentiation of fibroblasts into myofibroblasts plays a crucial role in the processes of granulation, collagen deposition, and wound contraction during dermis layer regeneration.[56] During the initiation of the ECM remodeling phase subsequent to the granulation phase, myofibroblasts undergo either apoptosis or redifferentiation into fibroblasts, resulting in their subsequent disappearance from the tissue. However, if myofibroblasts persist in the latent phase of the wound healing process, it can result in excessive contraction and eventually result in hypertrophic scars.[57] To determine the rate at which fibroblasts and myofibroblasts differentiate, α-smooth muscle actin (α-SMA)- and transforming growth factor β (TGF-β)-

https://doi.org/10.1021/acs.biomac.4c00406
Biomacromolecules XXXX, XXX, XXX−XXX

positive cells were quantified (Figure 7b,c) (n = 5). TGF-β is known to activate fibroblasts to differentiate into myofibroblasts, and myofibroblasts have been shown to express elevated levels of α-SMA. On day 7, the OGN-7 group demonstrated the highest number of α-SMA-positive and TGF-β-positive cells, suggesting a higher myofibroblast activity than the control and alginate groups. On day 14, the number of α-SMA and TGF-β-positive cells was lowest in the OGN-7 group, possibly due to a reduction in myofibroblasts from the accelerated resolution of the wound healing phase. In both the alginate and control groups, the number of α-SMA-positive and TGF-β-positive cells continued to rise at day 14, implying an ongoing phase of wound healing.

To confirm the extent of collagen transition during the ECM remodeling phase of the wound healing process, we performed immunofluorescent staining of collagen type I and collagen type III.[58] During wound regeneration, the initial granular tissue, which is predominantly composed of collagen type III, gets replaced by collagen type I to restore the skin's inherent flexibility and physical properties. Consequently, the transition from collagen III to collagen I is an important indicator of the maturation of regenerating skin. Collagen I deposition was greatest in the OGN-7 group on day 7 and was significantly higher than the control and alginate groups by day 14. This result is consistent with earlier findings from histological analysis, suggesting that OGN-7 accelerates the most deposition of collagen type I. On day 7, the expression of collagen type III was significantly higher in the OGN-7 group than in the control and alginate groups, indicating the early onset of the granulation phase. By day 14, both the alginate and OGN-7 groups exhibited a substantial decrease in collagen type III, suggesting that the skin was maturing toward collagen type I, which is comparable to the mature skin composition (Figure S11), with the OGN-7 group displaying a greater expression of collagen type I. This result indicates that OGN-7 enhances collagen maturation and wound healing capabilities.

In vivo analysis demonstrated that OGN-7 has the ability to promote wound healing by substantially boosting cellular activity in comparison to the alginate hydrogel, a widely used wound dressing material. Furthermore, it has the potential to promote the maturation of collagen in regenerated skin tissue, restoring its mechanical and biological properties to their normal state.

The outstanding *in vivo* outcomes of OGN-7 can be attributed to the three constituent elements of OGN-7, gelatin, OA, and nanofiber. Gelatin, a hydrolyzed form of collagen, closely resembles the natural collagen of the skin, exhibiting excellent cell affinity for numerous regenerative cells such as fibroblasts, keratinocytes, and macrophages.[2] This compatibility is crucial for enhancing various cellular processes, including proliferation, migration, and differentiation, making gelatin an ideal material for wound healing applications. However, the weak mechanical properties of gelatin restrict its clinical application when utilized alone.[59] Alginate possesses commendable physical properties but is hindered by the absence of motifs that facilitate cell attachment, leading to a lack of cellular interactions.[2,60] This limitation significantly impedes the material's biodegradation by cells during the wound healing process, consequently obstructing wound closure. Such restrictions not only delay wound closure but also interfere with critical healing stages such as re-epithelialization and granulation, ultimately slowing the overall rate of tissue regeneration. To address these challenges, OGN-7 was engineered to overcome the individual drawbacks of its components. We have modified oxidized alginate to significantly increase its biodegradation rate through ring-opening reactions, preventing it from hindering the wound closure process and accelerating re-epithelialization. Furthermore, by cross-linking gelatin with oxidized alginate via the Schiff-base reaction, we have enhanced the intrinsically weak mechanical properties of gelatin. This modification allows for the sustained enhancement of the wound regeneration capabilities of gelatin at the injury site, providing long-term benefits.[8] Furthermore, the incorporation of PCL/gelatin-based nanofibers into the hydrogel has enhanced its overall structural stability. This allows the wound to be covered throughout the wound regeneration process and creates an optimal environment for enhanced cellular activity, resulting in a more pronounced therapeutic impact compared to alginate wound dressings.

4. CONCLUSIONS

This paper describes the development of an injectable and remendable hydrogel consisting of OA, gelatin, and PCL/gelatin nanofibers. The OGN-7 hydrogel has superior mechanical, remending, and gelling capabilities due to the dual cross-linking through the Schiff-base reaction. According to our optimizations, the ideal concentration of the PCL/gelatin nanofiber was 5 mg/mL nanofiber consisting of 7:3 ratio of PCL/gelatin, which showed an excellent modulus, injectability, and cytocompatibility. A full-thickness *in vivo* wound healing analysis demonstrated that OGN-7 could achieve an enhanced level of wound closure and re-epithelialization. Overall, OGN-7 can overcome the limitations of natural polymer-based wound dressings and upregulate its regeneration-promoting properties, suggesting new possibilities in the field of wound dressings.

■ ASSOCIATED CONTENT

Supporting Information

The Supporting Information is available free of charge at https://pubs.acs.org/doi/10.1021/acs.biomac.4c00406.

List of antibodies, average fiber diameter, water contact angle of PCL/gelatin nanofibers, distribution of axial lengths of nanofiber fragments, gelation time, swelling ratio of hydrogels, SEM image of hydrogels, strain amplitude sweep test of OGN, stretch assay, histological staining of normal skin, and immunofluorescent staining of normal skin (PDF)

OGN-7 achieving full fusion and maintaining structural integrity under external stress (MP4)

■ AUTHOR INFORMATION

Corresponding Authors

Sang-Heon Kim − *Center for Biomaterials, Biomedical Research Institute, Korea Institute of Science and Technology (KIST), 02792 Seoul, Republic of Korea; Division of Bio-Medical Science and Technology, KIST School, University of Science and Technology (UST), Seoul 02792, Republic of Korea*; Email: skimbrc@kist.re.kr

Kangwon Lee − *Department of Applied Bioengineering, Graduate School of Convergence Science and Technology, Seoul National University, Seoul 08826, Republic of Korea; Research Institute for Convergence Science, Seoul National University, Seoul 08826, Republic of Korea*; orcid.org/0000-0001-5745-313X; Email: kangwonlee@snu.ac.kr

https://doi.org/10.1021/acs.biomac.4c00406
Biomacromolecules XXXX, XXX, XXX−XXX

Authors

Changgi Hong − *Department of Applied Bioengineering, Graduate School of Convergence Science and Technology, Seoul National University, Seoul 08826, Republic of Korea; Program in Nanoscience and Technology, Graduate School of Convergence Science and Technology, Seoul National University, Seoul 08826, Republic of Korea;* orcid.org/0000-0003-4324-1392

Haeun Chung − *Center for Biomaterials, Biomedical Research Institute, Korea Institute of Science and Technology (KIST), 02792 Seoul, Republic of Korea; Division of Bio-Medical Science and Technology, KIST School, University of Science and Technology (UST), Seoul 02792, Republic of Korea*

Gyubok Lee − *Department of Applied Bioengineering, Graduate School of Convergence Science and Technology, Seoul National University, Seoul 08826, Republic of Korea;* orcid.org/0000-0001-6634-7523

Dongwoo Kim − *Department of Applied Bioengineering, Graduate School of Convergence Science and Technology, Seoul National University, Seoul 08826, Republic of Korea*

Zhuomin Jiang − *Department of Applied Bioengineering, Graduate School of Convergence Science and Technology, Seoul National University, Seoul 08826, Republic of Korea*

Complete contact information is available at: https://pubs.acs.org/10.1021/acs.biomac.4c00406

Author Contributions

#C.H. and H.C.: indicate first authors. C.H.: conceptualization, methodology, data curation, visualization, writing—original draft, and writing—review and editing. H.C.: data analysis, investigation, methodology, visualization, and writing—review and editing. G.L.: resources and formal analysis. D.K. software and validation. Z.J.: data curation and validation. S.-H.K.: supervision and funding acquisition. K.L.: supervision, funding acquisition, and project administration.

Funding

This research was funded by the Korea Health Industry Development Institute of the Ministry of Health & Welfare (grant number: HI22C139400) and in part by the Research Institute for Convergence Science. This research was supported by a grant of the Ministry of Trade, Industry and Energy, Republic of Korea (no. 20018522). This research was also funded by the Korea Institute of Science and Technology (2E33151).

Notes

The authors declare no competing financial interest.

REFERENCES

(1) Zhong, Y. J.; Xiao, H. N.; Seidi, F.; Jin, Y. C. Natural Polymer-Based Antimicrobial Hydrogels without Synthetic Antibiotics as Wound Dressings. *Biomacromolecules* **2020**, *21* (8), 2983−3006.

(2) Sheokand, B.; Vats, M.; Kumar, A.; Srivastava, C. M.; Bahadur, I.; Pathak, S. R. Natural polymers used in the dressing materials for wound healing: Past, present and future. *J. Polym. Sci.* **2023**, *61* (14), 1389−1414.

(3) Tavakoli, M.; Labbaf, S.; Mirhaj, M.; Salehi, S.; Seifalian, A. M.; Firuzeh, M. Natural polymers in wound healing: From academic studies to commercial products. *J. Appl. Polym. Sci.* **2023**, *140* (22), No. e53910, DOI: 10.1002/app.53910.

(4) Liang, Y. P.; Chen, B. J.; Li, M.; He, J. H.; Yin, Z. H.; Guo, B. L. Injectable Antimicrobial Conductive Hydrogels for Wound Disinfection and Infectious Wound Healing. *Biomacromolecules* **2020**, *21* (5), 1841−1852.

(5) Talebian, S.; Mehrali, M.; Taebnia, N.; Pennisi, C. P.; Kadumudi, F. B.; Foroughi, J.; Hasany, M.; Nikkhah, M.; Akbari, M.; Orive, G.; et al. Self-Healing Hydrogels: The Next Paradigm Shift in Tissue Engineering? *Adv. Sci.* **2019**, *6* (16), No. 1801664, DOI: 10.1002/advs.201801664.

(6) Qu, J.; Zhao, X.; Liang, Y. P.; Zhang, T. L.; Ma, P. X.; Guo, B. L. Antibacterial adhesive injectable hydrogels with rapid self-healing, extensibility and compressibility as wound dressing for joints skin wound healing. *Biomaterials* **2018**, *183*, 185−199.

(7) Chen, T.; Chen, Y. J.; Rehman, H. U.; Chen, Z.; Yang, Z.; Wang, M.; Li, H.; Liu, H. Z. Ultratough, Self-Healing, and Tissue-Adhesive Hydrogel for Wound Dressing. *ACS Appl. Mater. Interfaces* **2018**, *10* (39), 33523−33531.

(8) Balakrishnan, B.; Joshi, N.; Jayakrishnan, A.; Banerjee, R. Self-crosslinked oxidized alginate/gelatin hydrogel as injectable, adhesive biomimetic scaffolds for cartilage regeneration. *Acta Biomater.* **2014**, *10* (8), 3650−3663.

(9) Balakrishnan, B.; Mohanty, M.; Umashankar, P. R.; Jayakrishnan, A. Evaluation of an in situ forming hydrogel wound dressing based on oxidized alginate and gelatin. *Biomaterials* **2005**, *26* (32), 6335−6342.

(10) Sarker, A.; Amirian, J.; Min, Y. K.; Lee, B. T. HAp granules encapsulated oxidized alginate-gelatin-biphasic calcium phosphate hydrogel for bone regeneration. *Int. J. Biol. Macromol.* **2015**, *81*, 898−911.

(11) Xuan, H. Y.; Wu, S. Y.; Fei, S. M.; Li, B. Y.; Yang, Y. M.; Yuan, H. H. Injectable nanofiber-polysaccharide self-healing hydrogels for wound healing. *Mater. Sci. Eng., C* **2021**, *128*, No. 112264, DOI: 10.1016/j.msec.2021.112264.

(12) Qiu, W. W.; Han, H.; Li, M. N.; Li, N.; Wang, Q.; Qin, X. H.; Wang, X. L.; Yu, J. Y.; Zhou, Y. X.; Li, Y.; et al. Nanofibers reinforced injectable hydrogel with self-healing, antibacterial, and hemostatic properties for chronic wound healing. *J. Colloid Interface Sci.* **2021**, *596*, 312−323.

(13) Cheng, K. C.; Huang, C. F.; Wei, Y.; Hsu, S. H. Novel chitosan-cellulose nanofiber self-healing hydrogels to correlate self-healing properties of hydrogels with neural regeneration effects. *NPG Asia Mater.* **2019**, *11*, No. 25, DOI: 10.1038/s41427-019-0124-z.

(14) Li, X. F.; Yang, Q.; Zhao, Y. J.; Longa, S. J.; Zheng, J. Dual physically crosslinked double network hydrogels with high toughness and self-healing properties. *Soft Matter* **2017**, *13* (5), 911−920.

(15) Eftekhari, A.; Dizaj, S. M.; Ahmadian, E.; Przekora, A.; Khatibi, S. M. H.; Ardalan, M.; Vahed, S. Z.; Valiyeva, M.; Mehraliyeva, S.; Khalilov, R.; et al. Application of Advanced Nanomaterials for Kidney Failure Treatment and Regeneration. *Materials* **2021**, *14* (11), No. 2939, DOI: 10.3390/ma14112939.

(16) Azarsa, S.; Pezeshki-Modaress, M.; Yazdian, F.; Bagher, Z.; Chahsetareh, H.; Simorgh, S.; Heidari, M. K.; Davachi, S. M. Nanofiber/hydrogel composite scaffolds based on alginate sulfate and extracellular matrix for cartilage tissue engineering applications. *Process Biochem.* **2024**, *136*, 60−71.

(17) Ahmadian, E.; Eftekhari, A.; Janas, D.; Vahedi, P. Nanofiber scaffolds based on extracellular matrix for articular cartilage engineering: A perspective. *Nanotheranostics* **2023**, *7* (1), 61−69.

(18) Pardo, A.; Gomez-Florit, M.; Davidson, M. D.; Öztürk-Öncel, M. Ö.; Domingues, R. M. A.; Burdick, J. A.; Gomes, M. E. Hierarchical Design of Tissue-Mimetic Fibrillar Hydrogel Scaffolds. *Adv. Healthcare Mater.* **2024**, No. 2303167, DOI: 10.1002/adhm.202303167.

(19) Yu, W.; Zhang, X. Q.; Gu, M. G.; Wang, J. Y.; Zhang, Y. H.; Zhang, W. K.; Yuan, W. E. Bioactive Nanofiber-Hydrogel Composite Regulates Regenerative Microenvironment for Skeletal Muscle Regeneration after Volumetric Muscle Loss. *Adv. Healthcare Mater.* **2024**, No. 2304087, DOI: 10.1002/adhm.202304087.

(20) Balakrishnan, B.; Lesieur, S.; Labarre, D.; Jayakrishnan, A. Periodate oxidation of sodium alginate in water and in ethanol-water mixture: a comparative study. *Carbohydr. Res.* **2005**, *340* (7), 1425−1429.

(21) Emami, Z.; Ehsani, M.; Zandi, M.; Foudazi, R. Controlling alginate oxidation conditions for making alginate-gelatin hydrogels (vol 198, pg 509, 2018). *Carbohydr. Polym.* **2019**, *208*, 200.
(22) Hong, C.; Chung, H.; Lee, G.; Kim, C.; Kim, D.; Oh, S. J.; Kim, S. H.; Lee, K. Hydrogel/Nanofiber Composite Wound Dressing Optimized for Skin Layer Regeneration through the Mechanotransduction-Based Microcellular Environment. *ACS Appl. Bio Mater.* **2023**, *6*, 1774−1786, DOI: 10.1021/acsabm.3c00014.
(23) Jiang, Z.; Nguyen, B. T. D.; Seo, J.; Hong, C.; Kim, D.; Ryu, S.; Lee, S.; Lee, G.; Cho, Y. H.; Kim, J. F.; et al. Superhydrophobic polydimethylsiloxane dip-coated polycaprolactone electrospun membrane for extracorporeal membrane oxygenation. *J. Membr. Sci.* **2023**, *679*, No. 121715, DOI: 10.1016/j.memsci.2023.121715.
(24) Choi, Y.; Park, M. H.; Lee, K. Injectable thermoresponsive hydrogel/nanofiber hybrid scaffolds inducing human adipose-derived stem cell chemotaxis. *J. Ind. Eng. Chem.* **2020**, *82*, 89−97.
(25) Pettignano, A.; Haring, M.; Bernardi, L.; Tanchoux, N.; Quignard, F.; Diaz, D. D. Self-healing alginate-gelatin biohydrogels based on dynamic covalent chemistry: elucidation of key parameters. *Mater. Chem. Front.* **2017**, *1* (1), 73−79.
(26) Gautam, S.; Dinda, A. K.; Mishra, N. C. Fabrication and characterization of PCL/gelatin composite nanofibrous scaffold for tissue engineering applications by electrospinning method. *Mater. Sci. Eng., C* **2013**, *33* (3), 1228−1235.
(27) Lu, B. L.; Lin, F. C.; Jiang, X.; Cheng, J. J.; Lu, Q. L.; Song, J. B.; Chen, C.; Huang, B. One-Pot Assembly of Microfibrillated Cellulose Reinforced PVA-Borax Hydrogels with Self-Healing and pH-Responsive Properties. *ACS Sustainable Chem. Eng.* **2017**, *5* (1), 948−956.
(28) Park, H.; Guo, X.; Temenoff, J. S.; Tabata, Y.; Caplan, A. I.; Kasper, F. K.; Mikos, A. G. Effect of Swelling Ratio of Injectable Hydrogel Composites on Chondrogenic Differentiation of Encapsulated Rabbit Marrow Mesenchymal Stem Cells In Vitro. *Biomacromolecules* **2009**, *10* (3), 541−546.
(29) Thomas, J.; Sharma, A.; Panwar, V.; Chopra, V.; Ghosh, D. Polysaccharide-Based Hybrid Self-Healing Hydrogel Supports the Paracrine Response of Mesenchymal Stem Cells. *ACS Appl. Bio Mater.* **2019**, *2* (5), 2013−2027.
(30) Kang, K.; Ye, S.; Jeong, C.; Jeong, J.; Ye, Y. S.; Jeong, J. Y.; Kim, Y. J.; Lim, S.; Kim, T. H.; Kim, K. Y.; et al. Bionic artificial skin with a fully implantable wireless tactile sensory system for wound healing and restoring skin tactile function. *Nat. Commun.* **2024**, *15* (1), No. 10, DOI: 10.1038/s41467-023-44064-7.
(31) Zhou, L.; Dai, C.; Fan, L.; Jiang, Y. H.; Liu, C.; Zhou, Z. N.; Guan, P. F.; Tian, Y.; Xing, J.; Li, X. J.; et al. Injectable Self-Healing Natural Biopolymer-Based Hydrogel Adhesive with Thermoresponsive Reversible Adhesion for Minimally Invasive Surgery. *Adv. Funct. Mater.* **2021**, *31* (14), No. 2007457, DOI: 10.1002/adfm.202007457.
(32) Pereira, R.; Carvalho, A.; Vaz, D. C.; Gil, M. H.; Mendes, A.; Bartolo, P. Development of novel alginate based hydrogel films for wound healing applications. *Int. J. Biol. Macromol.* **2013**, *52*, 221−230.
(33) Nezhad-Mokhtari, P.; Ghorbani, M.; Roshangar, L.; Rad, J. S. A review on the construction of hydrogel scaffolds by various chemically techniques for tissue engineering. *Eur. Polym. J.* **2019**, *117*, 64−76.
(34) Ruehl, M.; Somasundaram, R.; Schoenfelder, I.; Farndale, R. W.; Knight, C. G.; Schmid, M.; Ackermann, R.; Riecken, E. O.; Zeitz, M.; Schuppan, D. The epithelial mitogen keratinocyte growth factor binds to collagens via the consensus sequence glycine-proline-hydroxyproline. *J. Biol. Chem.* **2002**, *277* (30), 26872−26878.
(35) Jang, J.; Lee, J.; Seol, Y. J.; Jeong, Y. H.; Cho, D. W. Improving mechanical properties of alginate hydrogel by reinforcement with ethanol treated polycaprolactone nanofibers. *Composites, Part B* **2013**, *45* (1), 1216−1221.
(36) Sun, L. Y.; Gao, W. D.; Fu, X. L.; Shi, M.; Xie, W. H.; Zhang, W.; Zhao, F. J.; Chen, X. F. Enhanced wound healing in diabetic rats by nanofibrous scaffolds mimicking the basketweave pattern of collagen fibrils in native skin. *Biomater. Sci.* **2018**, *6* (2), 340−349.
(37) Xu, Y.; Shi, G. D.; Tang, J. C.; Cheng, R. Y.; Shen, X. F.; Gu, Y.; Wu, L.; Xi, K.; Zhao, Y. H.; Cui, W. G.; et al. ECM-inspired micro/nanofibers for modulating cell function and tissue generation. *Sci. Adv.* **2020**, *6* (48), No. eabc2036, DOI: 10.1126/sciadv.abc2036.
(38) Yang, Z. F.; Wang, C.; Zhang, Z. Y.; Yu, F. Z.; Wang, Y.; Ding, J. Q.; Zhao, Z.; Liu, Y. C. A pH responsive tannic acid/quaternized carboxymethyl chitosan/oxidized sodium alginate hydrogels for accelerated diabetic wound healing and real-time monitoring. *Int. J. Biol. Macromol.* **2024**, *264*, No. 130741, DOI: 10.1016/j.ijbiomac.2024.130741.
(39) Guo, Y. J.; Wang, X. Y.; Li, B. B.; Shen, Y.; Shen, L. Y.; Wu, J. X.; Yang, J. Oxidized sodium alginate crosslinked silk fibroin composite scaffold for skin tissue engineering. *J. Biomed. Mater. Res., Part B* **2022**, *110* (12), 2667−2675.
(40) Naghizadeh, Z.; Karkhaneh, A.; Khojasteh, A. Self-crosslinking effect of chitosan and gelatin on alginate based hydrogels: Injectable in situ forming scaffolds. *Mater. Sci. Eng., C* **2018**, *89*, 256−264.
(41) Baniasadi, H.; Mashayekhan, S.; Fadaoddini, S.; Haghirsharifzamini, Y. Design, fabrication and characterization of oxidized alginate-gelatin hydrogels for muscle tissue engineering applications. *J. Biomater. Appl.* **2016**, *31* (1), 152−161.
(42) Balakrishnan, B.; Mohanty, M.; Fernandez, A. C.; Mohanan, P. V.; Jayakrishnan, A. Evaluation of the effect of incorporation of dibutyryl cyclic adenosine monophosphate in an in situ-forming hydrogel wound dressing based on oxidized alginate and gelatin. *Biomaterials* **2006**, *27* (8), 1355−1361.
(43) Jejurikar, A.; Seow, X. T.; Lawrie, G.; Martin, D.; Jayakrishnan, A.; Grondahl, L. Degradable alginate hydrogels crosslinked by the macromolecular crosslinker alginate dialdehyde. *J. Mater. Chem.* **2012**, *22* (19), 9751−9758.
(44) Resmi, R.; Parvathy, J.; John, A.; Joseph, R. Injectable self-crosslinking hydrogels for meniscal repair: A study with oxidized alginate and gelatin. *Carbohydr. Polym.* **2020**, *234*, No. 115902, DOI: 10.1016/j.carbpol.2020.115902.
(45) Ko, Y. G.; Kwon, O. H. Reinforced gelatin-methacrylate hydrogels containing poly(lactic-co-glycolic acid) nanofiber fragments for 3D bioprinting. *J. Ind. Eng. Chem.* **2020**, *89*, 147−155.
(46) Lee, S. J.; Kim, H. J.; Heo, M.; Lee, H. R.; Choi, E. J.; Kim, H.; Lee, D.; Reis, R. L.; Do, S. H.; Kwon, I. K. In vitro and in vivo assessments of an optimal polyblend composition of polycaprolactone/gelatin nanofibrous scaffolds for Achilles tendon tissue engineering. *J. Ind. Eng. Chem.* **2019**, *76*, 173−180.
(47) Jiang, Y. C.; Wang, X. F.; Xu, Y. Y.; Qiao, Y. H.; Guo, X.; Wang, D. F.; Li, Q.; Turng, L. S. Polycaprolactone Nanofibers Containing Vascular Endothelial Growth Factor-Encapsulated Gelatin Particles Enhance Mesenchymal Stem Cell Differentiation and Angiogenesis of Endothelial Cells. *Biomacromolecules* **2018**, *19* (9), 3747−3753.
(48) Shim, W. S.; Yoo, J. S.; Bae, Y. H.; Lee, D. S. Novel injectable pH and temperature sensitive block copolymer hydrogel. *Biomacromolecules* **2005**, *6* (6), 2930−2934.
(49) Joorabloo, A.; Khorasani, M. T.; Adeli, H.; Mansoori-Moghadam, Z.; Moghaddam, A. Fabrication of heparinized nano ZnO/poly(vinylalcohol)/carboxymethyl cellulose bionanocomposite hydrogels using artificial neural network for wound dressing application. *J. Ind. Eng. Chem.* **2019**, *70*, 253−263.
(50) Chen, M. H.; Wang, L. L.; Chung, J. J.; Kim, Y. H.; Atluri, P.; Burdick, J. A. Methods To Assess Shear-Thinning Hydrogels for Application As Injectable Biomaterials. *ACS Biomater. Sci. Eng.* **2017**, *3* (12), 3146−3160.
(51) Varaprasad, K.; Jayaramudu, T.; Kanikireddy, V.; Toro, C.; Sadiku, E. R. Alginate-based composite materials for wound dressing application:A mini review. *Carbohydr. Polym.* **2020**, *236*, No. 116025, DOI: 10.1016/j.carbpol.2020.116025.
(52) Son, Y. J.; Tse, J. W.; Zhou, Y. R.; Mao, W.; Yim, E. K. F.; Yoo, H. S. Biomaterials and controlled release strategy for epithelial wound healing. *Biomater. Sci.* **2019**, *7* (11), 4444−4471.
(53) Li, Z.; Song, J. B.; Zhang, J. F.; Hao, K. G.; Liu, L.; Wu, B. Q.; Zheng, X. Y.; Xiao, B.; Tong, X. L.; Dai, F. Y. Topical application of silk fibroin-based hydrogel in preventing hypertrophic scars. *Colloids Surf., B* **2020**, *186*, No. 110735, DOI: 10.1016/j.colsurfb.2019.110735.

https://doi.org/10.1021/acs.biomac.4c00406
Biomacromolecules XXXX, XXX, XXX−XXX

(54) Guo, S.; DiPietro, L. A. Factors Affecting Wound Healing. *J. Dent. Res.* **2010**, *89* (3), 219−229.
(55) Hu, C.; Chu, C. Y.; Liu, L.; Wang, C. B.; Jin, S. E.; Yang, R. L.; Rung, S. A.; Li, J. D.; Qu, Y. L.; Man, Y. Dissecting the microenvironment around biosynthetic scaffolds in murine skin wound healing. *Sci. Adv.* **2021**, *7* (22), No. eabf0787, DOI: 10.1126/sciadv.abf0787.
(56) Darby, I. A.; Laverdet, B.; Bonte, F.; Desmouliere, A. Fibroblasts and myofibroblasts in wound healing. *Clin., Cosmet. Invest. Dermatol.* **2014**, *7*, 301−311.
(57) Gauglitz, G. G.; Korting, H. C.; Pavicic, T.; Ruzicka, T.; Jeschke, M. G. Hypertrophic Scarring and Keloids: Pathomechanisms and Current and Emerging Treatment Strategies. *Mol. Med.* **2011**, *17* (1−2), 113−125.
(58) Xue, M. L.; Jackson, C. J. Extracellular Matrix Reorganization During Wound Healing and Its Impact on Abnormal Scarring. *Adv. Wound Care* **2015**, *4* (3), 119−136.
(59) Zhang, H.; Lin, X.; Cao, X. Y.; Wang, Y.; Wang, J. L.; Zhao, Y. J. Developing natural polymers for skin wound healing. *Bioact. Mater.* **2024**, *33*, 355−376.
(60) Cao, Y.; Cong, H. L.; Yu, B.; Shen, Y. Q. A review on the synthesis and development of alginate hydrogels for wound therapy. *J. Mater. Chem. B* **2023**, *11* (13), 2801−2829.

https://doi.org/10.1021/acs.biomac.4c00406
Biomacromolecules XXXX, XXX, XXX−XXX